Unconventional filling dynamics of a pit crater

manuscript submitted to *Earth and Planetary Science Letters*

Unconventional filling dynamics of a pit crater

P.-Y. Burgi[1*], S. Valade[2], D. Coppola[3], G. Boudoire[4,], G. Mavonga[5], F. Rufino[6], and D. Tedesco[6,7,8,9]

[1] IT Department, University of Geneva, 1211 Genève, Switzerland.

[2] Departamento de Vulcanología, Instituto de Geofísica, Universidad Nacional Autónoma de México, Mexico City, Mexico.

[3] Dipartimento di Scienze della Terra, Università di Torino, Torino, Italia.

[4] Laboratoire Magmas et Volcans, UCA, CNRS, IRD, OPGC, 63178 Aubière, France.

[5] Observatoire Volcanologique de Goma, Goma, RDC.

[6] Università degli Studi della Campania "Luigi Vanvitelli", DiSTABIF, 81100 Caserta, Italia.

[7] Istituto Nazionale Geofisica e Vulcanologia, Osservatorio Vesuviano, Via Diocleziano, Napoli, Italia.

[8] European Union Delegation, Kinshasa, DRC – Bruxelles, European Union.

[9] MONUSCO (United Nations)- Goma, Democratic Republic of Congo.

* Corresponding author Pierre-Yves Burgi (pierre-yves.burgi@unige.ch)

Abstract

The rise and fall of magma columns is a process commonly observed in volcanoes hosting lava lakes and serves as proxy of magmatic reservoir pressure and warning for potential eruptions. This dynamic process typically involves the filling and emptying of a “pit crater” - a cylindrical depression usually formed by one or more collapses of a structure lying above an emptied surficial reservoir. Between 2016 and 2020, the 300 m deep pit crater located within Nyamulagira volcano (Democratic Republic of Congo) underwent an unusual filling dynamic. In May 2019 while filled to about 90% the crater floor collapsed by 90 m within two months, followed by the rapid emergence of a sub-

circular solidified block overlooking the crater rim in less than 6 months. Using numerical simulations of models based on thermal energy and constrained by multiparametric data, we account for the incremental filling of the crater by successive intra-crateric lava flows and the subsequent collapse of the crater floor. We further characterize this unconventional filling mode based on thermal budget considerations.

Keywords: volcano; remote sensing; pit crater; lava lake; thermal model, thermal budget

1. Introduction

Pit craters are common features on basaltic volcanoes (Harris, 2009), defined as cylindrical depressions with steeply inward dipping sides usually formed by one or more collapses of a structure lying above an associated emptied surficial reservoir. Their evolution is closely related to near surface magmatic activity (Walker, 1988). Pit craters may or may not be occupied by lava lakes. Those lava lakes may be active, fed from depth and usually persistent over substantial period of time. Their level within the crater vary in accordance to pressure changes at the base of a convecting magmatic column (Burgi et al., 2020, 2002; Coppola et al., 2016a; Duffell et al., 2003; Lev et al., 2019; Patrick et al., 2019; Valade et al., 2018). Inactive lava lakes are in turn accounted for by lavas erupted from active vents inside or outside the pit crater, spreading intermittent lava flows within it (Harris, 2009; Swanson et al., 1979). Termination of magma supply will cause the entrapped lava layers to gradually cool and solidify.

While the dynamic of active (convective) lava lakes have been extensively modelled (e.g., Harris, 2008), the emplacement of inactive lava lakes still lack a dedicated model able to explain the complex dynamics of filling, emptying and solidification operating within these structures (e.g., Harris, 2009). The two filling dynamics (active and inactive), may produce similar surface structures

making the recognition of one mechanism rather than another not trivial. However, the two mechanisms are likely characterized by different ratio between the thermal energy radiated by the lake surface, and the volumetric growth rate inside the pit crater. In fact, active lava lakes radiate much more thermal energy than that contained in the lava that eventually accumulates on the surface (Coppola et al., 2013). This is because the convective magma column allows the hot magma to rise, degas and loose heat, before most of it is cycled back into the system (Burgi et al., 2020, 2002). The extreme case is visible in stable, long-lived lava lakes that emit a considerable amount of heat without increasing its volume (e.g. Erta Ale, Erebus, Nyiragongo during stable phases, Harris et al., 1999). On the contrary, inactive lava lakes, being basically fed by an effusive activity, are characterized by thermal emissions that are proportional to the volume of erupted lava (Coppola et al., 2013; Harris and Baloga, 2009), without any additional contribution due to convective processes.

In this study we report the evolution of a new lava lake which appeared inside a summit pit crater of Nyamulagira (Democratic Republic of Congo) in 2014 (Fig. 1c). Ground and satellite observations (see methodology) have made it possible to track the filling dynamic of the pit crater by measuring the volume of lava accumulating inside, as well as the net discharge rate (Q_{out}) and the volcanic radiant power associated to the surface activity (VRP). These observations highlight the occurrence of distinct phases of rise of the pit-crater floor, that cannot be accounted exclusively by one of the above-mentioned models, but rather by a transition from active to inactive filling mechanism. Moreover, during the phase of inactive lava lake emplacement, we observe the subsidence of the pit-crater floor, followed by the uplift of a solidified basaltic block whose dynamics

shares typical aspects of both the subsidence and resurgence of solid blocks observed in caldera-forming eruptions.

We thus focus on the peculiar filling-emptying-filling dynamics characterizing the inactive lava lake stage between 2016 and 2020, and we propose a thermal model (fed by remote-sensed data) whereby successive intra-crater lava flows pile up at different rates to produce layers of lava with different states of solidification. On this basis, our model is able to explain the complex pit-crater evolution recently observed at Nyamulagira which include the unusual subsidence and block uplift, rarely observed at mafic calderas (Galetto et al., 2019; Geist et al., 2006a).

2. Nyamulagira setting

Nyamulagira is the westernmost volcano of the Virunga Volcanic Province (Democratic Republic of Congo - DRC) in the western branch of the East African Rift System (EARS) (Fig. 1a). It is a predominantly mafic shield volcano with a 3058-m-high summit caldera, a diameter of more than 2 km, and one of the most active volcanoes of the EARS (Bluth and Carn, 2008). As many basaltic shield volcanoes, Nyamulagira is mostly characterized by frequent flank eruptions, with a total of 40 occurrences from the summit crater and from its flanks over the last 120 years (Michellier et al., 2020; Pouclet and Bram, 2021). The presence of a lava lake has also been documented in 1930-1938 (Wadge and Burt, 2011) and its drainage in 1938 has led to the longest (more than 2 years) and most voluminous (>200 x 10^6 m^3) historical eruptive event (Pouclet, 1975; Wadge and Burt, 2011), with lava flows rapidly reaching Lake Kivu located 25 km downstream. The very end of the 2011–2012 peripheral eruption was marked by a co-eruptive explosive collapse of a pit crater floor in the caldera's north-eastern sector. After a period of 74 years (R. Hoier, 1939) a new lava lake was firstly observed in 2014 (Campion, 2014; Coppola et al., 2016a; Smets et al., 2015, 2014), occupying the bottom of this pit crater estimated between 400 and 500 m deep. This pit crater has

93 now almost (not always) lost its frequent use as a lava lake container and seems to represent the
94 central (superficial) part of Nyamulagira's plumbing system (Pouclet and Bram, 2021; Wauthier et
95 al., 2013).

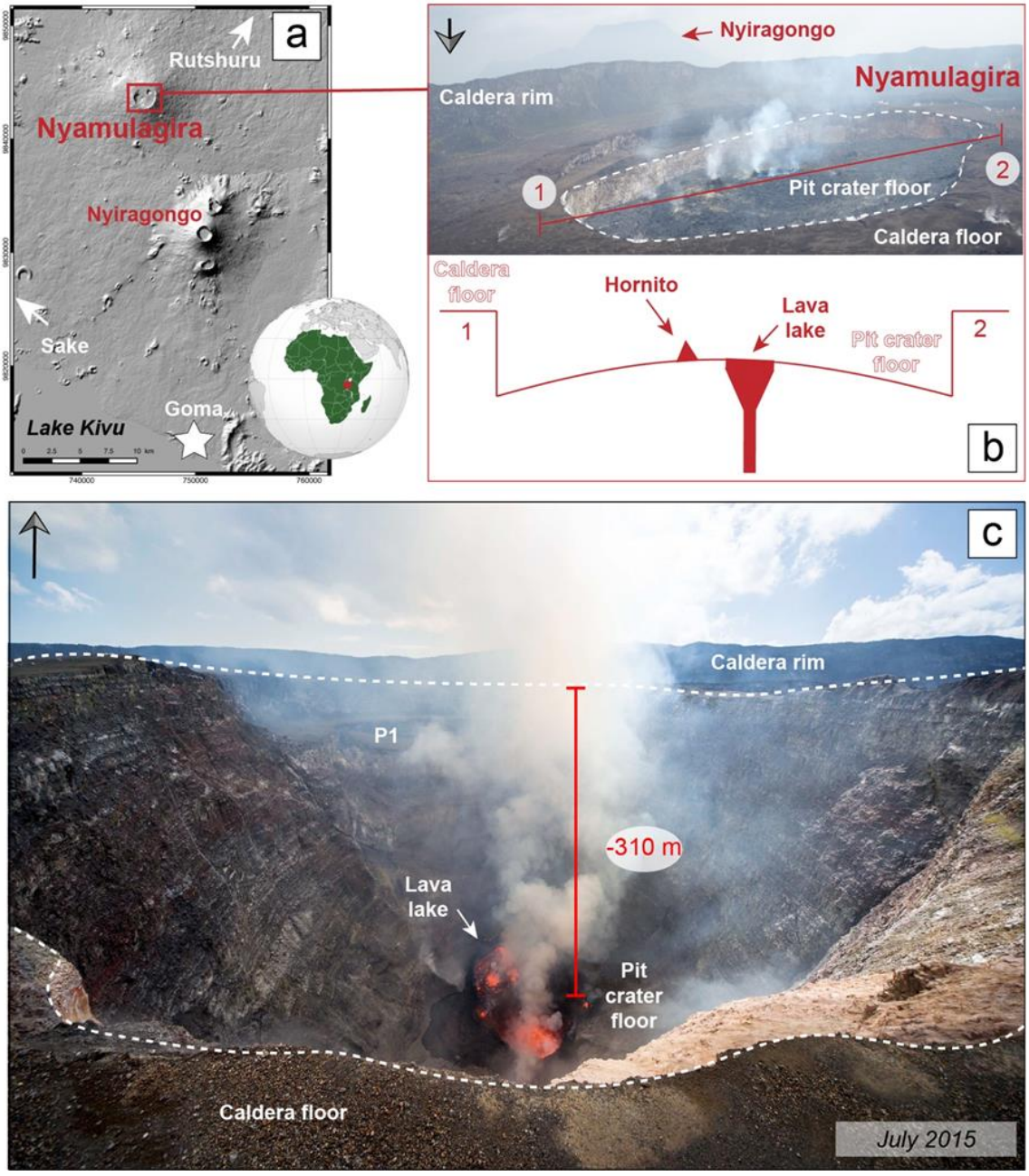

96

Fig. 1. Setting of the pit crater. (a) Location of Nyamulagira and Nyiragongo (another active volcano), and the City of Goma. Digital Elevation Model (DEM) computed from the Shuttle Radar Topography Mission (SRTM, 2000) data extracted from USGS Earth Explorer. (b) Aerial image on February 18, 2019 pointing out the morphology of the pit crater at Nyamulagira along with cross section schematically illustrated (vertical scale exaggerated). At this time the pit crater was about 600 m long and 400 m wide and was almost completely filled. (c) The pit crater in July 2015. Pictures from the authors.

3. Methodology

3.1 Data Acquisition

Periodic field surveys inside the Nyamulagira caldera were carried out between November 2014 and February 2020 with the support of the Observatoire Volcanologique de Goma (OVG) and the MONUSCO (United Nations Organization Stabilization Mission in DRC). During each mission (from a few hours to several days), a comprehensive series of field observations and measurements were conducted to document the physical configuration of the active pit crater, using Laser Range Finder Binoculars. These field campaigns were supplemented by helicopter observations performed by MONUSCO whenever they could fly over this region. which made it possible to estimate the pit-crater floor level at different states of its evolution with an accuracy of about 10% of the absolute value.

These estimations were complemented by Sentinel-1 Synthetic-Aperture Radar (SAR) images processed by the MOUNTS volcano monitoring system (Valade et al., 2019) (www.mounts-project.com) to measure both the pit-crater depth evolution and the caldera deformation, from January 2018 to June 2020. Depth is calculated from the intensity image, by measuring the length of the shadow casted by the pit crater walls in radar geometry, and multiplying it by the cosine of the radar incidence angle (Wadge et al., 2011). The method has successfully been applied to track lava lake level variations (Barrière et al., 2018; Moore et al., 2019), and here provides continuous

variations of the pit-crater floor, which are validated by sporadic field measurements. Deformation is calculated from standard differential SAR interferometry analysis (D-InSAR), with interferograms computed with the shortest temporal baseline, i.e., between two consecutive acquisitions (typically 6-day interval on the ascending track, and 12-days interval on the descending track). Unwrapping of the interferograms was done with SNAPHU to recover ground deformation in the radar line-of-sight (LOS) in meters. The ground and satellite data relating to the depth of the pit crater were used to calculate the volume of lava accumulating inside the pit crater (assuming an inverted truncated cone geometry with r_{min}= 113 m and r_{max}= 250 m; Fig. 2a). Volumetric estimates have been finally used to calculate growth rate (Q_{out}) for each analyzed period (Fig. 2b).

Thermal emissions have been detected using infrared data provided by the moderate resolution imaging spectroradiometer (MODIS), compiled within the Middle InfraRed Observation of Volcanic Activity (MIROVA) system (Coppola et al., 2016b; www.mirovaweb.it) to facilitate their analysis and determine the volcanic radiative power (VRP; Fig. 2c). The MODIS data were supported by the images acquired from the Copernicus Sentinel 2 sensors (resolution of 20 m in the short-wave infrared - SWIR bands), which made it possible to identify in greater spatial detail the high temperature areas at the origin of the measured heat flux.

4. Observations and measurements

4.1 Pit-crater filling dynamic between 2014 and 2020

First observations of a lava lake inside the summit pit-crater of Nyamulagira date back to mid-2014 (Coppola et al., 2016b) when visual observations confirmed the presence of fresh magma (~50 m diameter) lava lake at the bottom of the pit-crater (~500 m depth). In July 2015, the lava lake displayed an elliptical shape, 150 m long and 100 m wide, and was located at a depth of 310 m

below the crater rim (Fig. 1c). This initial phase of activity (volume less than 2 x 10^6 m^3) was followed by a period without any evidence of lava lake activity (Supp. Fig. S1a) until December 2016, when the pit crater started to be filled by fresh lava. The new vigorous filling phase led the pit crater floor to rise at a depth of 160 m below the crater rim, with a diameter of ~190 m and a volume of ~14 x 10^6 m^3 by May 2017 (Supp. Fig. S1b). A new phase of rest occurred between June 2017 and May 2018 when the third filling phase started (see next section). Overall, the volume of lava accumulated in the pit-crater from April 2014 to April 2020 amounts to approximately 37 x 10^6 m^3 with an average magma output rate of 0.18 m^3/s (Fig. 2a). This volume of lava accounts for only 12% of the long-term magma output rate of Nyamulagira between 1980 and 2012 (~1.5 m^3/s; Coppola et al., 2016a; Fig. 2b).

The three main phases of lava lake growth are well highlighted by the cumulative volume trend as well as by the evolution of the lava discharge rate (Q_{out}) and by the VRP (Fig. 2). As anticipated in the introduction the ratio between thermal flux (VRP) and volumetric growth rate (Q_{out}), hereby defined as c_{rad}= VRP/Q_{out} (Coppola et al., 2013) is a parameter representing the amount of heat radiated into the atmosphere for each cubic meter of lava erupted or accumulated inside the crater (Fig. 2d). c_{rad} outlines how the three phases represented in Fig. 2a, were characterized by markedly different values (Fig. 2d), likely associated to distinct mechanism of lava lake formation (see Introduction). The first phase (May 2014 to May 2016) was characterized by c_{rad}> 10^9 J/m^3 (Fig. 2d), a value much higher than the one typically measured during the flank lava-flow-forming eruption of Nyamulagira 2-5 x 10^8 J/m^3 (Coppola and Cigolini, 2013; red field in Fig. 2d). We ascribe this phase to the development of an active lava lake, whereby the excess of radiation is associated to the convective circulation of magma at shallow depth. Conversely the second (December 2016 to May 2017) and third (April 2018 to April 2020) filling phases were characterized by a c_{rad} similar to, if not even smaller than, the typical value characterizing the effusive regime. This is likely due

to the absence of magma convection and to the limited surface area of lava flows confined within the pit, the thickness of which is controlled by geometric, rather than rheological, factors (Harris and Baloga, 2009). Accordingly, we ascribe these two phases to the intermittent growth of an inactive lava lake (blue field in Fig. 2d) whose detailed morphological evolution is described in the next section and modelled in section 5.

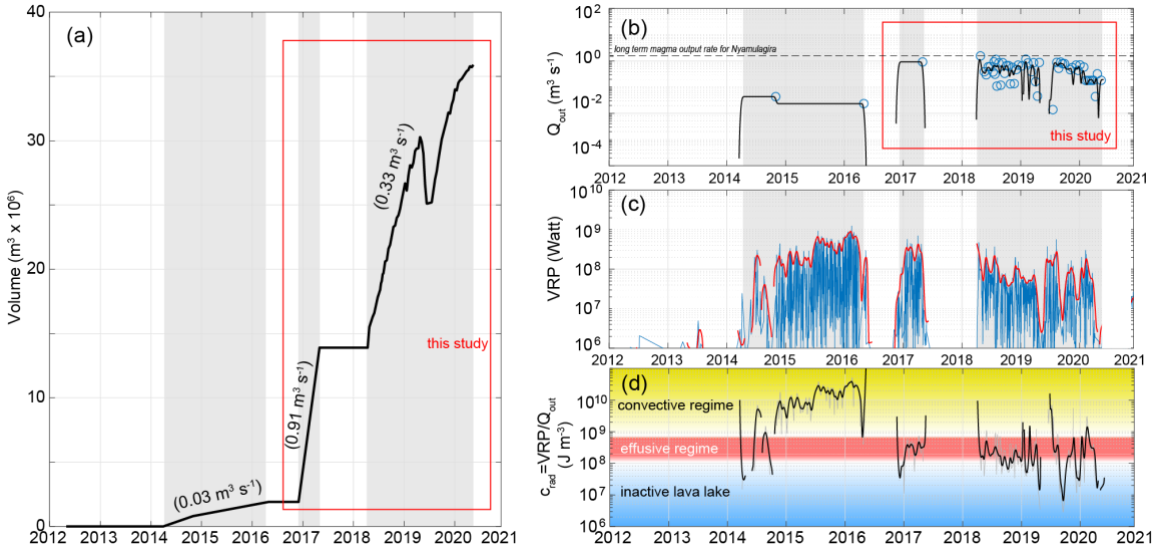

Fig. 2. (a) Cumulative volume of lava emplaced inside the summit crater of Nyamulagira between the first appearance of a lava lake, in 2014 (Coppola et al., 2016a) and mid-2020. Three main growth phases (grey fields) are defined by the respective time-averaged lava discharge rate (in parenthesis). (b) The lava output rate (Q_{out}) associated to each phase is compared to the long-term magma output rate (1.5 m^3/s) that characterized Nyamulagira effusive activity between 1980-2012 (Aoki et al., 1985; Coppola et al., 2016a). (c) Volcanic Radiative Power (VRP) associated to the three phases, as measured by the MIROVA system. (d) ratio between the radiant and

182 volumetric flux (c_{rad}=VRP/Q_{out}) throughout the analyzed period. Yellow and blue colored fields
183 refer to active and inactive lava lake mechanisms, respectively.

184 **4.2 Pit-crater activity between 2018-2020**

185 The third phase of growth (2018-2020), on which we focus in this study, was characterized by a
186 complex dynamic which we subdivided into three stages.

187 *4.2.1 Filling of the pit-crater (May 2018 – April 2019: Rise 1 phase)*

188 In May 2018 MIROVA thermal anomalies were suddenly detected after a nearly 1-year hiatus, and
189 the level of the pit-crater floor began to rise at a steady rate, as evidenced by the Sentinel-1 SAR
190 analysis (Fig. 3a,d) and field measurements.

191 Ground observations in July and November 2018 put in evidence intra-crateric lava flows taking
192 their origin either from a small lava lake (when present) or from hornitos (Fig. 4a,b & Supp. Fig.
193 S2). In February 2019, the small lava lake was located at the top of a convex surface that occupied
194 the whole crater and dominated the bottom of the cliffs from a height of about 15 m (Figs. 1b & 4b).

At this time, lava flows could be observed at the base of the pit-crater cliffs and occurred nearly continuously during our 5-day stay (Fig. 4b).

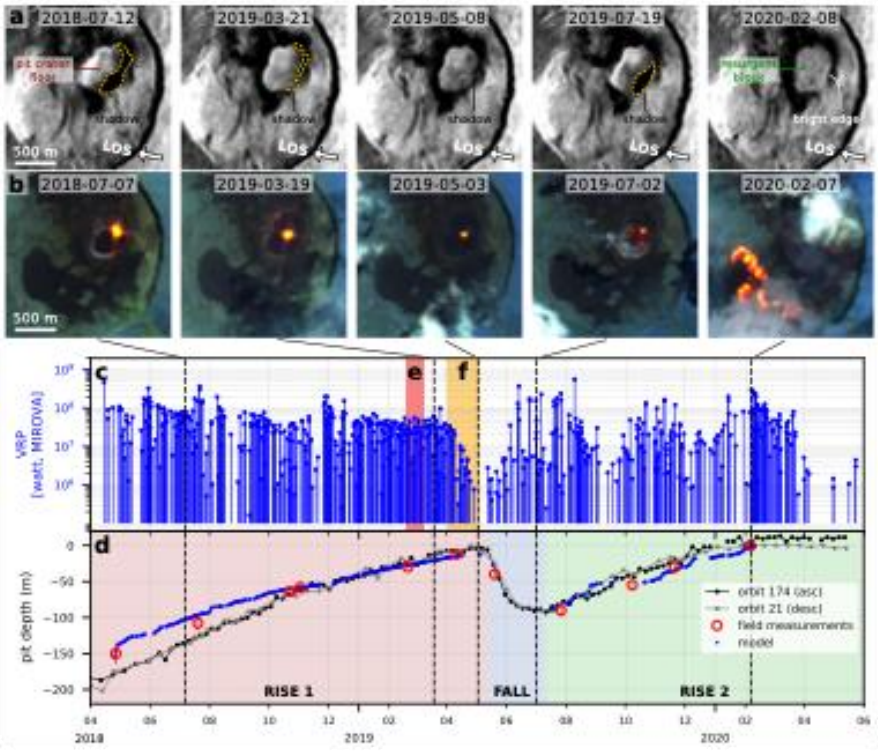

Fig. 3. Multiparametric data analysis. (a) Sentinel-1 SAR acquired in descending orbit (orbit 21, line-of-sight LOS represented by white arrow), geocoded and speckle-filtered. The variations of the shadow casted inside the pit crater (dashed yellow lines) highlight the variations of the crater depth. (b) Sentinel-2 SWIR bands 12-11-8A. (c) Volcanic Radiative Power (VRP) measured from MODIS TIR images (processed by MIROVA). (d) Pit crater depth estimated from field measurements (red markers), Sentinel-1 SAR images with ascending and descending orbits in black and gray respectively (processed by MOUNTS), and lava layers thickness modeling (blue line). The 3 phases corresponding to the filling (Rise 1), emptying (Fall), and re-filling (Rise 2) of the pit-crater are highlighted in red, blue and green respectively (as in Figure 4). (e) Timespan indicating when deformation was measured by InSAR following a dyke intrusion under the caldera (Supp. Fig. S3). (f) Timespan indicating a period when the thermal radiation decreased significantly, evidenced by a drop in the VRP values and a decrease of the active lava lake dimensions.

From January 2019 to June 2019, tectonic seismicity around the Nyamulagira area shallower than 20 km was recorded by the seismic network of the Goma Volcanology Observatory (GVO). Many

inhabitants have reported experiencing earthquakes in the North (mostly from the City of Rutchuru, located 35 km from Nyamulagira), and South of Nyamulagira, particularly in the lake Kivu area, including the Goma City, with magnitudes up to 4.5. In February 2019, deformation inside the crater was detected in three distinct interferograms, spanning from February 13 to March 9, 2019 (Fig. 3e). The InSAR deformation pattern suggests that a dyke firstly propagated from the pit crater towards the South-East and accumulated under the most eastern-side of the caldera floor (Supp. Fig. S3). No lava emissions were associated with this deformation episode, which resulted in a maximum deformation in the radar line-of-sight of 8.4 cm. Shortly afterwards, the thermal activity within the crater dropped significantly from April 12, 2019 to early May 2019 (Fig. 3f), as testified by the decrease in VRP detections. Notably, the decrease in the lava lake size (which was 50 m long and 30 m wide at the end of February 2019), and the disappearance of lava flows surrounding the crater floor, visible already in July 2018 (Fig. 3b) were not accompanied by the subsidence of the pit-crater floor but rather, by a slow upward rise (Fig. 3d).

4.2.2 Subsidence of the pit-crater (May 2019 – June 2019: Fall phase)

A radical change in the crater activity occurred in May 2019 with a large subsidence of the pit-crater floor lasting 2 months (Fig. 3d, "Fall" phase). The first ground-based observation of this phenomenon dates back to May 2019 with a floor subsiding by about 10 m with respect to its level two months before. While no direct observations were reported, both MONUSCO, which makes regular reconnaissance flights in this area, and local inhabitants reported rumbling and smoke from inside the crater, that could correspond to the floor's detachment. MONUSCO also reported that a camp inhabited for more than 10 years by a rebel group on the southern upper flank of the volcano was suddenly abandoned in the second half of May 2019. However, as the closest seismic station is 25 km away, the event did not yield discernible seismic signals, with the exception of two long-

period (LP) seismic swarms in May 8-9, 2019 and in May 16-19, 2019, which could be linked to the first phases of the sinking of the pit-crater floor.

This subsidence reached -90 m at the end of July 2019 (Fig. 4c), representing a loss of a volume of lava of about 8 x 10^6 m^3. No fractures of the pit-crater floor nor at its surroundings or outside the crater on its flanks were observed, as it usually occurs during caldera collapses at basaltic shield volcanoes (Derrien et al., 2020; Neal et al., 2019). The morphology of the pit crater floor with the hornito in its center stayed surprisingly intact and kept degassing (Figure 4c). Two platforms located in the northern part of the pit crater (P1 and P2, Fig. 1c), which had been covered with a lava layer estimated to be 35 m thick during the filling of the pit crater in 2018, were cleared and became partly visible again (Fig. 4c).

4.2.3 Re-filling of the pit-crater and uplift of a solidified block (July 2019 – February 2020: Rise 2 phase)

Following the subsidence phase, the pit-crater floor resumed rising at the end of July 2019 (Rise 2 phase), with the emplacement of lava flows at the bottom of the pit (Fig. 4c). Shortly after, the bottom of the pit-crater appeared as a sub-circular 290 m x 390 m solidified block as attested by the development of a large fracture (Fig. 4d & Supp. Fig. S4). This solidified block stayed intact throughout this re-filling phase (fracture still visible in the 2020-03-03 satellite image, Fig. 4e & Supp. Fig. S5a), suggesting that the block was being pushed from below similar to a piston-mechanism, with an uplift rate in the order of cm per hour. In February 2020, the pit crater was completely filled and lava was overflowing from its periphery onto the main caldera floor (Fig. 4e & Supp. Fig. S5). At this time, the emergent solidified block protruded about 10 m above the caldera floor (Fig. 4e). This protruded topography was also observable on Sentinel-1 SAR images, as the pit-crater edge no longer appeared as a dark shadow (i.e. negative topography), but rather as a

thin bright edge, indicating the reflection of the radar electromagnetic wave onto a positive topography (Fig. 3a).

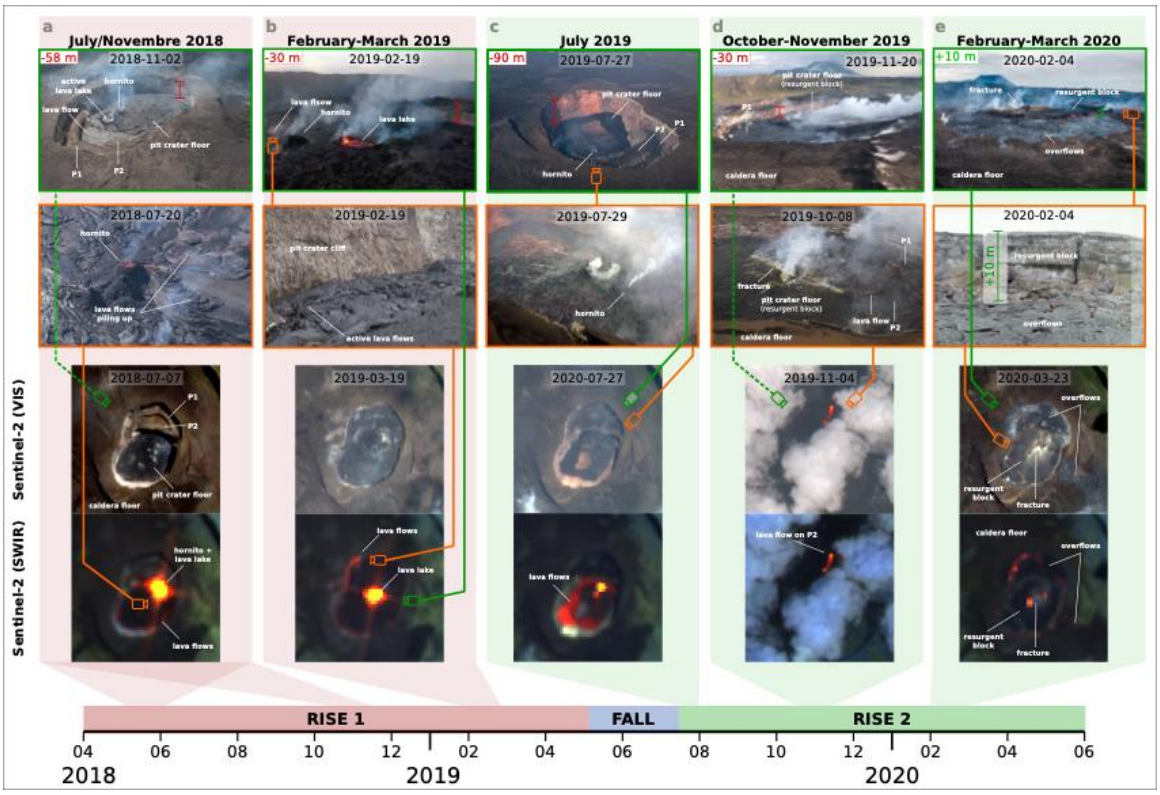

Fig. 4. Evolution of the pit crater morphology from April 2018 to June 2020 based on photographs and satellite images (Sentinel-2, optical and SWIR band combinations). The 3 phases corresponding to the pit-crater filling (Rise 1), emptying (Fall), and re-filling (Rise 2) are respectively represented in red, blue, and green (as in Fig. 3). Pictures from the authors.

5 Numerical Models

Based on the above-described multiparametric data, modeling was used to explain (i) the filling of the pit crater, (ii) the subsidence that followed without evidence of brittle fracturing, (iii) the emergence of a solidified block, and (iv) the state of crystallization of the successive layers based on a thermal model. Note that only the period preceding subsidence (April 2016 to April 2019, Supp.

Fig. S1) is considered for the thermal model, as “rise 2” phase involves a piston effect not fully accountable by a thermal model.

5.1 Lava layer thickness

We model the filling of the Nyamulagira crater from April 2016 to February 2020 not as a rising lava lake, but rather as the stacking of a succession of distinct lava flows detected remotely by the MIROVA system. We apply the following relation between the radiative energy *VRE* and the erupted volume *V* (Coppola et al., 2013),

$$c_{rad} = \frac{VRE\ \gamma}{V} \qquad (1)$$

where γ is a correction factor (set to 1.3) for compensating the thermal energy attenuation due to the presence of clouds (frequent in this region), and c_{rad} is the radiant density, which characterizes several properties of the lava emplacement, such as insulation, rheological and topographic conditions. The particular geological context of these flow units (lava flows confined in a deep crater) implies that, for a fixed effusion rate, these intra-crater lava flows will have a smaller surface area than equivalent lava flows that are emplaced along the flank of the volcano (free to expand). For the case of caldera confined lava emplacement, the thickness of the lava layers at day *n* may be approximated by $H_n = V_n/(\pi r^2)$, with *r* the average pit crater radius. From equation (1), which takes into account all radiative sources, including the presence of a small lava lake, we can express the layer’s thickness H_n as

$$H_n = \frac{VRE_n\ H_{tot}}{VRE} \qquad (2)$$

with H_{tot} being the total lava flow thickness, and VRE_n corresponding to the radiative energy calculated for each specific day *n*. To avoid unrealistic lava flows, a thickness smaller than 10 cm

is discarded. Consequently, the time separating two lava flows is determined by the occurrence of layers thicker than this threshold value.

5.2 Collapsing conditions

According to visual observations performed in July 2019 (Fig. 4c), the floor's detachment has occurred along a pit-crater segment with sub-vertical cliffs. We thus model it as a vertical piston whose load is balanced by friction at the wall surrounding it. Also, the condition for a solid portion of height H_s in contact with pit-crater walls to collapse is satisfied when the vertical load (F_v) (Duputel and Rivera, 2019; Kumagai, 2001)

$$F_v = \frac{\pi D^2 H_s \rho g}{4} \qquad (3)$$

with *D* the average pit-crater diameter, ρ the density of degassed magma, and g the gravity acceleration, exceeds a critical shear force (F_s) given by (Roche and Druitt, 2001)

$$F_s = \tau_c \pi H_s D, \qquad (4)$$

where τ_c is the critical shear stress for rupture, taken to follow the Coulomb fracture criterion (Nicholson, 1994),

$$\tau_c = \tau_0 + \mu \frac{\nu}{1-\nu} \frac{\rho g H_s}{2}, \qquad (5)$$

with ν the Poisson's ratio and μ the sliding friction. Because the pit crater was filled by successive lava layers, and that lava may be oozing at the edges and thus lubricating some contact points, cohesion τ_0 is estimated to be 1-2 orders of magnitude lower than the value for intact basalt (Schultz, 1995). To be conservative, we set $\tau_0 = 1$ x 10^6 Pa. Combining the last three equations, the collapse condition $F_v > F_s$ is verified for

$$H_s < \frac{1-\nu}{\mu\upsilon}\left(\frac{D}{2} - \frac{2\tau_0}{\rho g}\right) \qquad (6)$$

With the parameters reported in Table 1, we estimate a total solid layer height $H_s < 423$ m. Later in Section 4.2 we show that the solid layers are all much smaller than this value, which indicates that the collapsing condition is always satisfied once the underlying pressure drops.

5.3 Heat equation

Based on ground observations (Fig. 4 & Supp. Fig. S2), we take for granted that magma erupts by successive lava flows, the initial one with thickness H_1 at liquidus temperature T_{liq}. By heat radiation and convection within the surrounding atmosphere T_{atm}, cooling of the lava surface starts and proceeds by conduction toward the lava interior, with latent heat released inside the lava layers due to crystallization. A new lava flow covers the previous layer with thickness H_2, and the process repeats until the crater is filled. The layer thickness H_n (equation 2) and the lava flows' occurrence time t_n are both evaluated based on the radiant density estimated from MIROVA data.

Temperature and melt fraction of the lava layers are computed using the finite difference expression of the heat equation. Given the horizontal spatial extent of the pit crater (several hundreds of meters) and duration of the considered period, we assume that the horizontal heat loss at the crater walls does not affect the vertical temperature distribution, and thus a one-dimensional model can be applied. This assumption is at least reasonable for the central part of the crater under study. To calculate the temporal and spatial evolution of temperature $T(X,t)$ of this central part that experiences repeated accumulation of lava flows, we apply the heat equation, derived by combining the conservation of energy and Fourier's law

$$k\frac{\partial^2 T}{\partial X^2} = \rho c_p \frac{\partial T}{\partial t} - \rho L \frac{\partial f_c}{\partial t} \qquad (7)$$

where (see Table 1) f_c is melt fraction (which depends on temperature), *k* is thermal conductivity, ρ is the density, c_p is specific heat capacity, *L* is latent heat, *t* is time, and X is vertical distance, which increases after each lava flow.

To best match available data on the rheology of Nyamulagira's lavas (Morrison et al., 2020), variation of the crystallinity with temperature *T* is approximated by a nonlinear function,

$$f_c = a + bsinh(c\frac{T-T_{sol}}{T_{liq}-T_{sol}} + d) \quad (8)$$

with T_{sol} the solidus temperature, which for many magmas is observed to correspond to $T_{liq} - 200$ (Marsh, 1981; Wright and Marsh, 2016), and T_{liq} is set to 1260 ºC (Morrison et al., 2020). This function yields slow crystallization within the first 80-100 ºC subliquidus, and then changes regime with a fast increase in the rate of crystallization. While the absolute temperature of this interval shifts to lower temperatures with decreasing oxygen fugacity, the width of this temperature interval remains similar (Kolzenburg et al., 2020, 2018a). Substituting this definition for f_c in equation (7), we get

$$\frac{\partial^2 T}{\partial X^2} = \frac{\partial^2 T}{\partial X^2} = \frac{\rho}{k}\left[c_p - \frac{L\,b\,c}{T_{liq}-T_{sol}}cosh(c\frac{T-T_{sol}}{T_{liq}-T_{sol}} + d)\right]\frac{\partial T}{\partial t} \quad (9)$$

with parameters *a*, *b*, *c* and *d* in Table 1. With the chosen parameters, the "cut-off" temperature where crystallization exponentially increases (Kolzenburg et al., 2016) is at 1180 ºC. The heat flux from the lava surface ($X = 0$) is described by a boundary condition, which we take

$$\sigma\varepsilon(T^4 - T_{atm}^4) - k\frac{\partial T}{\partial x} = 0 \quad (10)$$

where the first term stands for the radiant heat flux, with σ the Stefan-Boltzmann constant and ε the emissivity of the lava surface, and the second term stands for heat transfer by conduction. It must be noted that we neglected heat transfer by natural convection in this equation as heat lost

by radiant heat flux is several orders of magnitude larger for the range of considered temperatures. On the other hand, latent heat, liberated as lava solidifies, has a significant effect and provides a large quantity of energy per unit mass that delays cooling.

To keep computation time reasonable, equations (9) and (10) were discretized on a spatial mesh of 2.5 cm (the thinnest lava flow being 10 cm) and time increment fixed to 8 minutes. These settings verify the mesh Fourier number criterion (Smith et al., 1985): for the considered heat equation this criterion is given by $F = \frac{k}{\rho c_p} \Delta t / \Delta x^2$, which yields 0.49, verifying the stability condition F < 0.5. At the occurrence of each lava flow, whose time of occurrence and thickness (see above) were derived from the MIROVA data, the equation is reinitialized with new initial and boundary conditions, which corresponds to instantaneously emplaced lava.

Table 1 HERE. Physical properties and parameters employed in the model.

6 A stratified pit crater highlighted by numerical modeling

The numerical solutions of the thermal model (vertical thermal profile) during the April 2016 - April 2019 period, reveal that just before the subsidence occurred in May-June 2019, the pit crater consisted of an alternation of molten and solidified layers (Fig. 5b). Of the 290 m of lava piled up during this period, about 160 m were solidified (cf. S1 to S5 on Fig. 5b) and 130 m were in a molten state (cf. M1-M4 on Fig. 5b). The preservation of molten layers results mainly from the effect of the latent heat generated during the cooling and solidification of other layers. Without this effect, almost the entire pit crater would be solidified (Supp. Fig. S6). We argue that molten layers interspersed between solid layers promote the collapse of the crater and accelerate the phenomenon (by draining the molten layers – Fig. 5c). On contrary, the displacement of a 300 m rock thickness will generate much more friction against the wall. While being conservative in the values of equation 6,

a thickness of 300 m is closer to the limit value (423 m), which might potentially be overvalued. Moving thinner solid layers more easily meets the dropout condition.

The layer thickness evolution (described by equation 2 and inferred from MIROVA) closely fits the field and satellite observations (Fig. 3b & Supp. Fig. S7) although the 2-3 m individual layers (middle panel of Fig. 4e) and Supplementary Figure S4a cannot be resolved through the heat equation solutions (e.g., Fig. 5b). This would have required the inclusion of layer boundary formation mechanisms and intra-layer vertical variations (grain size, mineral compositions, textures, etc. present in the layers) in the model that involve a wide variety of factors (Naslund and McBirney, 1996), which was not the focus of this study.

Because thermal parameters are rarely provided for specific volcanoes, and Nyamulagira is not an exception, a sensitivity analysis was used to confirm the consistency of the results obtained (Table 1). No appreciable effect on the distribution of the solid layers in the stacked column have been observed (Supp. Fig. S8), and the predominant variables turn out to be the timing and thickness of the lava flow, both derived from MIROVA data. A similar observation has been reported for incremental intrusions in sills in which the rate of basalt emplacement (represented here by the timing and thickness of the lava flows) is an important variable in determining melt fraction (Annen, 2011; Jackson et al., 2018).

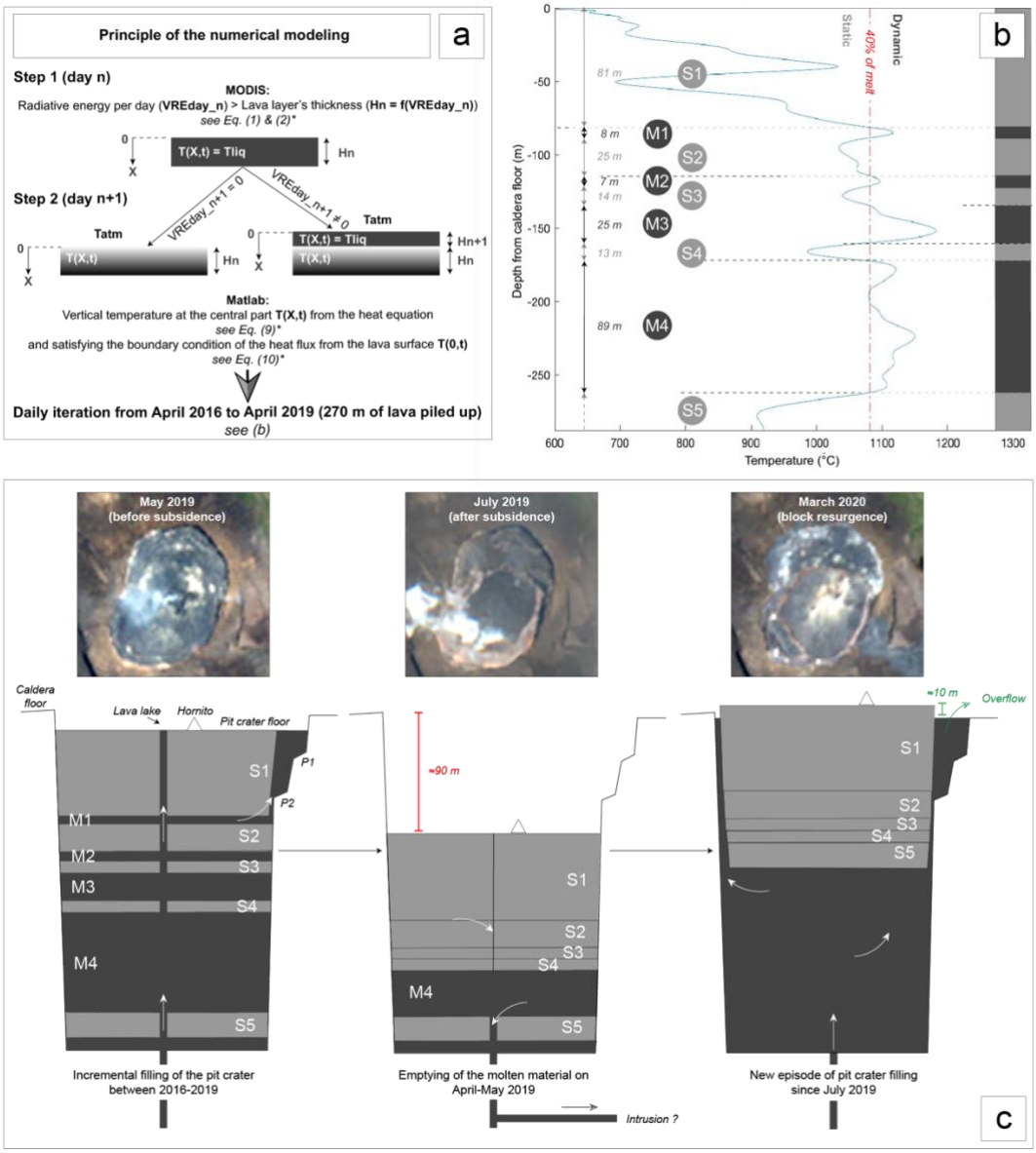

394

395 **Fig. 5.** Thermal modelling with the resulting collapse and emergence of the solid block scenario.
396 (a) Description of the main principles used in numerical modeling. Equations (*) are described in
397 Section 5. (b) Result of the numerical modeling (temperature profile) performed between April 2016
398 and April 2019 (about 1000 days) to simulate the state (S: solid vs. M: molten layers) of the pit
399 crater filled by 290 m of lava before its subsidence. The dashed red line indicates 40% melt fraction
400 (below this line the lava is supposed to be static and above it flowing). (c) Interpretative scheme
401 (not at scale) of the evolution of the pit crater before and after the subsidence (May 2019 - March
402 2020) together with Sentinel-2 images.

7 Discussion

The morphology of the pit crater and filling mode since April 2016 have led to the layering of lava with different states of solidification. The numerical solution of the thermal model (Fig. 5) shows that before the subsidence of May 2019 (i) a large part of the pit crater (~130 m) was filled with molten lava; (ii) the first 80 m upper segment of the pit crater is mostly solid, with a melt fraction smaller than 40%, and is thus too viscous to flow (Annen, 2011; Kolzenburg et al., 2018b; Lamy-Chappuis et al., 2020; Lejeune and Richet, 1995; Marsh, 1981; Sparks et al., 2019); (iii) under this solid crust reside several molten lava layers, the largest one being over 90 m thick, interspaced by solidified layers up to 25 m thick (Fig. 5b). We now discuss how this layer structure impacts the subsidence of the pit-crater (May – June 2019) and the following uplift of a solidified block (July 2019 - February 2020).

7.1 Subsidence and emergence mechanisms

Subsidence of the crater floor, which started in May 2019 and lasted 2 months (Fig. 3d), is most probably associated with lava draining from the shallow magmatic system. Although the origin of such draining is still unclear and outside the scope of this study, it is worth noting that this subsidence was preceded, 6 weeks before (in March 2019), by a small intrusion evidenced by InSAR (originating from the pit-crater and extending under the caldera floor, Supp. Fig. S3), concomitant to recorded tectonic earthquakes. Nevertheless, the intrusive episode was followed by a month-long reduction of the thermal flux (Figs. 2c & 3c) possibly indicating a break in the magmatic supply or a partial drainage of the magma column caused by the intrusion below the caldera floor. It should be noted that this decrease of magma supply to the surface did not cause the immediate collapse of the crater which began to subside only one month later, in early May 2019 (Fig. 3d). The following subsidence lowered the pit-crater floor of about 90 m (Figs. 3d & 4c),

426 a value that can be explained by our model as it corresponds to the drainage of almost all the
427 melted layers interspersed in the pit crater (Fig. 5c).

428 Ground observations suggest that the central part of the pit crater has sunk as a single solid block
429 (as a piston), a feature that makes this subsidence episode similar to a caldera collapse. Moreover,
430 the time delay between the observed deformation and subsidence is reminiscent of caldera
431 collapses where faulting can precede subsidence by several days to weeks (Derrien et al., 2020;
432 Shelly and Thelen, 2019).

433 Caldera collapses, with subsequent resurgence of domes, share similar characteristics with those
434 modeled here (Smith and Bailey, 1968): (i) Nyamulagira follows a piston model with a solid block
435 of plane-like and of sub-circular shape, where subsidence begins when gravity exceeds the
436 frictional forces with the surrounding wall rock (Duputel and Rivera, 2019; Kumagai, 2001; Michon
437 et al., 2011); (ii) fracturing of the subsiding blocks has been observed to depend on the ratio block's
438 thickness (T) to diameter (D) - in our case we estimate T/D=0.35, which tends to favor sagging as
439 a single central block subsidence (piston) style with well-defined ring faults, which would not be the
440 case for much thinner crust (for which T/D<0.3) (Holohan et al., 2013, 2011; Roche et al., 2000).
441 With such a thickness (160 m, Fig. 5c), the underlying magmatic column remains confined beneath
442 the crust, except for intrusions around the block, which was actually observed (panel July 27, 2019
443 in Figure S5B); (iii) uplift of a solid block is favored by a crystallized front, which serves as a
444 rheological barrier whereby magma intrusions accumulate and exerts an upward pressure (Galetto
445 et al., 2017); (iv) any subsequent increase in magma volume potentially causes surface volcanism
446 concomitantly with the uplift of the emergent block (or injection of magma into fracture systems);
447 (v) low-viscosity magma would tend to dissipate magma pressure adjacent to the emergent block
448 with consequent surface volcanism.

Besides the involved spatial scale much smaller than in caldera forming volcanic settings, two main differences can be highlighted: (1) subsidence is linked to the drainage of molten layers (Fig. 5c) in addition to the piston effect, which could accelerate subsidence; (2) uplift of the solid block occurred at a faster and constant rate of cm/hour instead of cm/year (Dvorak and Dzurisin, 1997; Geist et al., 2006; Métrich et al., 2011; Ukawa et al., 2006).

The uplift of the solid block formed by the compaction of the remaining solidified layers (Fig. 5c), which are lighter and cooler than the hottest and least differentiated magma (Sparks and Huppert, 1984), could be favored by an increase of the magma flow, and thus upward pressure. Taking the hydrostatic pressure $\rho g H$, where ρ and *H* are, respectively, the density and thickness of the solid block (Fig. 5c), and taking into account the friction force against the cliffs (equation 4), then about 7 MPa are required to make it resurface (the hydrostatic pressure counting for 60%). This represents an upper bound as most likely molten lava was interposed between the cliffs and the block (which explains the lava flows on the edge of the crater floor, e.g. Fig. 4), thereby reducing the frictional forces. The uplift of the solid block started in mid-July 2019 and was again accompanied by LP earthquake swarms at depth similar to those recorded in May 2019. Concomitant to the block uplift, fresh lavas flooded the area around it and finally overflowed the caldera floor in February 2020 (Fig. 4e and injection along the margins of the solidified surfaces on Supp. Fig. S5b).

According to Fig. 5c, there are no more interspaced molten layers and the whole piston is in contact with the magma column.

7.2 Towards an unconventional model of pit crater filling

The thermal model reveals a filling mechanism of the pit crater by successive solid and liquid layers whose thickness depends on frequency and size of the lava flows and size of the pit crater. This

filling pattern characterize the inactive lava lakes and is unconventional in the sense that it can be defined as alternative to both (1) a purely convective mode, where the convection disrupts solid layers (active lava lake, yellow zone on Fig. 2d) and (2) an effusive mode, where single flow units have time to solidify before stacking up (blue zone on Fig. 2d). This unconventional mode, which we call "streaky", is represented schematically in Fig. 6. Our model further highlights a filling mechanism that could occur in other craters. For example the neighboring Nyiragongo volcano, whose crater has been filled both by overflows of the lava lake (which also occupies only a portion of its floor surface) and by intra-crateric eruptions that began in 2016 with the formation of a new spatter cone (Burgi et al., 2020, 2018), shows great similitudes with Nyamulagira. However, no similar subsidence or block uplift has been observed, probably due to the different physical configuration of the crater and the underlying convective magma column.

Thermal models of discrete emplacement units of magma have previously been proposed to explain the formation of magma reservoirs and plutons (Annen, 2011; Annen and Sparks, 2002; Biggs and Annen, 2019; Blundy and Annen, 2016; Jackson et al., 2018; Michaut and Jaupart, 2011; Sparks et al., 2019). A common feature of these models is the magma emplacement modality, assumed to occur piecemeal with small increments rather than in a single large event. However, these thermal models are based on the following assumptions that are not applicable in our case: (i) successive magma injection through sills occurring upwards and downwards (Annen, 2011); (ii) the layers being intruded are not subject to radiative heat loss and cooling is mainly done by conductive loss; (iii) thick magma bodies may develop convective instabilities which accelerate cooling (Simakin and Trubitsyn, 1995); (iv) timescales are tens to hundreds of thousands of years, and spatial dimensions range on kilometer scale.

Solidification of lava lakes (Colp, 1982; Helz et al., 2014; Worster et al., 1993; Wright et al., 1976; Wright and Marsh, 2016), which starts once the magma influx needed to keep the molten state

496 strongly decreases or ceases, represents another situation governed by thermal equations similar
497 to those applied in our model. However, in the case of lava lake, the solidified surface crust
498 preventing further radiative heat loss and cooling is mainly controlled by heat transfer by conduction
499 to the host rocks, and through the upper crust of the lake to the air, corresponding to ε=0 in equation
500 (10). For stagnant lava ponds, such as the Kilauea inactive lava lakes (Wright et al., 1976), lava is
501 accumulated through successive eruptive phases. Also, crust solidification is much slower in lava
502 ponds than in our case: more than 7 years to solidify 80 m against less than 6 months in our case
503 (Helz et al., 2014; Wright et al., 1976). A common feature though is the density profile with depth,
504 where the cooled crust is lighter than the underlying hot melt.

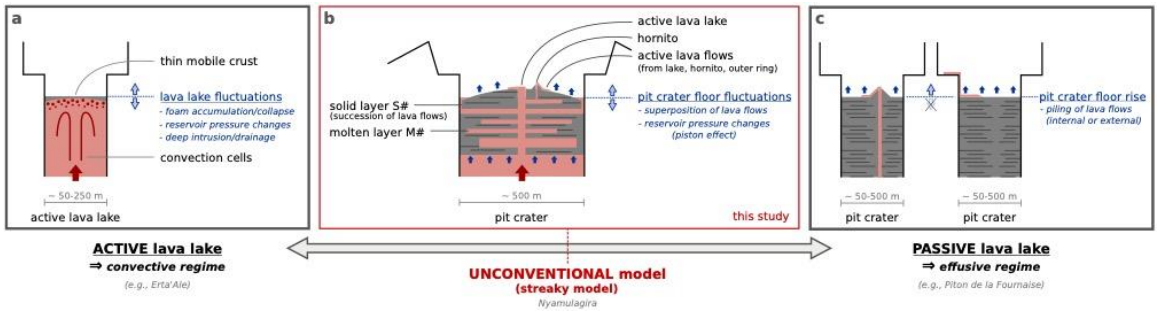

505

506 **Fig. 6.** Conceptual models used to explain depth variations of pit-craters. (a) Active lava lake model,
507 whereby the pit-crater hosts an active lava lake with convective cells: depth variations are
508 commonly explained by foam accumulation/collapse beneath a thin solid crust, and/or pressure
509 changes in the magma column/reservoir ("piston-effect"), and/or deep intrusion and magma column
510 drainage (Patrick et al., 2019). (b) Unconventional "streaky" model presented in this study, whereby
511 the pit-crater is filled by interleaved solid and molten layers: the depth fluctuations are explained by
512 both the piling of lava flows, and by variations of the magma column/reservoir pressure. (c) Passive
513 lava lake, whereby the pit-crater is filled passively by piling of lava flows from vents located inside

514 and/or outside the pit: the pit-crater floor does not fluctuate up/down, but only rises depending on
515 the effusive activity alone.

516 **4 Conclusions**

517 This case study, based on field and satellite measurements, and numerical modelling, shows a new
518 crater filling dynamic: while being in close contact with a magma column, Nyamulagira's pit crater
519 fills up incrementally by the overlapping of intra-crateric lava flows. This mechanism results in the
520 formation of solidified layers, interspersed with partially molten flow units, whose characteristics
521 depend on the temporal spacing between each emission of lava. Such an incremental filling of the
522 crater creates the conditions for the unconventional collapse and buoyant ascent of the solidified
523 layers, both of which constitute novel processes within pit craters. Our model thus contributes to
524 extend and improve our knowledge on processes underlying the dynamics of pit craters containing
525 lava lakes.
526 While the volcanic phenomena reported here are confined to the caldera, the underlying pressure
527 variations of the magmatic reservoir should be acknowledged as serious hazard for the region's
528 continuous population growth in the most western side of the Virunga Volcanic Province. Indeed,
529 lava flows generated by Nyamulagira directly threaten the city of Sake with a population of over
530 100,000 inhabitants (located 25 km from the volcano), and potentially lead to severe logistical
531 supply problems by cutting the only road that links Goma (the capital of North Kivu, population >1
532 million, located at about 30 km south east of the volcano) to the western and southern territories of
533 north and south Kivu (Balagizi et al., 2018; Patrick et al., 2019; Tedesco et al., 2007), as shown by
534 the recent event of the nearby Nyiragongo in May 2021.

535 **Acknowledgments**

This mission could not be done without the invitation of the Goma Volcano Observatory (OVG), their logistic help and their information provided on the activity of Nyamulagira. MONUSCO is warmly thanked for providing crucial support in several field deployments by helicopter in areas of unrest that are highly insecure. The Virunga National Parc (ICCN Institut Congolais pour la Conservation de la Nature) provided logistics inside the National Parc of Virunga and provided full assistance with their very professional rangers in the field. We also wish to thank Andrew Harris, Robin Campion, and Thomas Walter for their helpful comments on an early version of the manuscript, Hervé Sthioul and Fabien Cruchon for their contributions in 3D photogrammetry. We also warmly thank the reviewer Stephan Kolzenburg and an anonymous reviewer for their constructive comments. We acknowledge the INGV initiative LakeCarb, the French government IDEX-ISITE initiative 16-IDEX-0001 (CAP 20-25), as well as UNAM PAPIIT funding (project IA102221). The development of MOUNTS was funded by Geo.X (Research Network for Geosciences in Berlin and Potsdam), and Prof. Hellwich (Computer Vision and Remote Sensing, TU-Berlin) is warmly thanked for hosting the server in his department.

Code and Data Availability

All data generated or analyzed during this study are provided with this article, and are available at https://doi.org/10.26037/yareta:khivh7h2prgvxauarlckdo7awi

MIROVA data, and the associated codes for computing the thickness and time of occurrence of the lava flows, as well as thermal evolution of the lava layers are available at https://doi.org/10.26037/yareta:5futgivyezdw5gdqqfogybt3ky

Sentinel-1 and Sentinel-2 data used in this study are available and freely downloadable from the Copernicus Open Access Hub (https://scihub.copernicus.eu/).

References

Annen, C., 2011. Implications of incremental emplacement of magma bodies for magma differentiation, thermal aureole dimensions and plutonism–volcanism relationships. Tectonophysics 500, 3–10. https://doi.org/10.1016/j.tecto.2009.04.010

Annen, C., Sparks, R.S.J., 2002. Effects of repetitive emplacement of basaltic intrusions on thermal evolution and melt generation in the crust. Earth Planet. Sci. Lett. 203, 937–955. https://doi.org/10.1016/S0012-821X(02)00929-9

Aoki, K.-I., Yoshida, T., Yusa, K., Nakamura, Y., 1985. Petrology and geochemistry of the Nyamuragira volcano, Zaire. J. Volcanol. Geotherm. Res. 25, 1–28. https://doi.org/10.1016/0377-0273(85)90002-2

Balagizi, C.M., Kies, A., Kasereka, M.M., Tedesco, D., Yalire, M.M., McCausland, W.A., 2018. Natural hazards in Goma and the surrounding villages, East African Rift System. Nat. Hazards 93, 31–66. https://doi.org/10.1007/s11069-018-3288-x

Barrière, J., d'Oreye, N., Oth, A., Geirsson, H., Mashagiro, N., Johnson, J.B., Smets, B., Samsonov, S., Kervyn, F., 2018. Single-Station Seismo-Acoustic Monitoring of Nyiragongo's Lava Lake Activity (D.R. Congo). Front. Earth Sci. 6, 82. https://doi.org/10.3389/feart.2018.00082

Biggs, J., Annen, C., 2019. The lateral growth and coalesence of magma systems. Philos. Trans. R. Soc. Math. Phys. Eng. Sci. 377, 20180005. https://doi.org/10.1098/rsta.2018.0005

Blundy, J.D., Annen, C.J., 2016. Crustal Magmatic Systems from the Perspective of Heat Transfer. Elements 12, 115–120. https://doi.org/10.2113/gselements.12.2.115

Bluth, G.J.S., Carn, S.A., 2008. Exceptional sulfur degassing from Nyamuragira volcano, 1979–2005. Int. J. Remote Sens. 29, 6667–6685. https://doi.org/10.1080/01431160802168434

Burgi, P. -Y., Boudoire, G., Rufino, F., Karume, K., Tedesco, D., 2020. Recent Activity of Nyiragongo (Democratic Republic of Congo): New Insights From Field Observations and Numerical Modeling. Geophys. Res. Lett. 47. https://doi.org/10.1029/2020GL088484

Burgi, P.-Y., Caillet, M., Haefeli, S., 2002. Field temperature measurements at Erta'Ale Lava Lake, Ethiopia. Bull. Volcanol. 64, 472–485. https://doi.org/10.1007/s00445-002-0224-3

Burgi, P.-Y., Minissale, S., Melluso, L., Mahinda, C.K., Cuoco, E., Tedesco, D., 2018. Models of the Formation of the 29 February 2016 New Spatter Cone Inside Mount Nyiragongo. J. Geophys. Res. Solid Earth 123, 9469–9485. https://doi.org/10.1029/2018JB015927

589 Campion, R., 2014. New lava lake at Nyamuragira volcano revealed by combined ASTER and OMI
590 SO $_2$ measurements. Geophys. Res. Lett. 41, 7485–7492.
591 https://doi.org/10.1002/2014GL061808

592 Colp, J.L., 1982. Magma Energy Research Project. Sandia Natl. Lab. Albuq. N. M., Sandia Report
593 SAND82-2377 42.

594 Coppola, D., Campion, R., Laiolo, M., Cuoco, E., Balagizi, C., Ripepe, M., Cigolini, C., Tedesco, D.,
595 2016a. Birth of a lava lake: Nyamulagira volcano 2011–2015. Bull. Volcanol. 78, 20.
596 https://doi.org/10.1007/s00445-016-1014-7

597 Coppola, D., Cigolini, C., 2013. Thermal regimes and effusive trends at Nyamuragira volcano (DRC)
598 from MODIS infrared data. Bull. Volcanol. 75, 744. https://doi.org/10.1007/s00445-013-
599 0744-z

600 Coppola, D., Laiolo, M., Cigolini, C., Donne, D.D., Ripepe, M., 2016b. Enhanced volcanic hot-spot
601 detection using MODIS IR data: results from the MIROVA system. Geol. Soc. Lond. Spec.
602 Publ. 426, 181–205. https://doi.org/10.1144/SP426.5

603 Coppola, D., Laiolo, M., Piscopo, D., Cigolini, C., 2013. Rheological control on the radiant density
604 of active lava flows and domes. J. Volcanol. Geotherm. Res. 249, 39–48.
605 https://doi.org/10.1016/j.jvolgeores.2012.09.005

606 Derrien, A., Peltier, A., Villeneuve, N., Staudacher, T., 2020. The 2007 caldera collapse at Piton de
607 la Fournaise: new insights from multi-temporal structure-from-motion. Volcanica 3, 55–
608 65. https://doi.org/10.30909/vol.03.01.5565

609 Duffell, H.J., Oppenheimer, C., Pyle, D.M., Galle, B., McGonigle, A.J.S., Burton, M.R., 2003. Changes
610 in gas composition prior to a minor explosive eruption at Masaya volcano, Nicaragua. J.
611 Volcanol. Geotherm. Res. 126, 327–339. https://doi.org/10.1016/S0377-0273(03)00156-
612 2

613 Duputel, Z., Rivera, L., 2019. The 2007 caldera collapse of Piton de la Fournaise volcano: Source
614 process from very-long-period seismic signals. Earth Planet. Sci. Lett. 527, 115786.
615 https://doi.org/10.1016/j.epsl.2019.115786

616 Dvorak, J.J., Dzurisin, D., 1997. Volcano geodesy: The search for magma reservoirs and the
617 formation of eruptive vents. Rev. Geophys. 35, 343–384.
618 https://doi.org/10.1029/97RG00070

619 Galetto, F., Acocella, V., Caricchi, L., 2017. Caldera resurgence driven by magma viscosity
620 contrasts. Nat. Commun. 8, 1750. https://doi.org/10.1038/s41467-017-01632-y

Geist, D., Chadwick, W., Johnson, D., 2006. Results from new GPS and gravity monitoring networks at Fernandina and Sierra Negra Volcanoes, Galápagos, 2000–2002. J. Volcanol. Geotherm. Res. 150, 79–97. https://doi.org/10.1016/j.jvolgeores.2005.07.003

Harris, A.J.L., 2009. The pit-craters and pit-crater-filling lavas of Masaya volcano. Bull. Volcanol. 71, 541–558. https://doi.org/10.1007/s00445-008-0241-y

Harris, A.J.L., 2008. Modeling lava lake heat loss, rheology, and convection: MODELING LAVA LAKE HEAT LOSS, RHEOLOGY, AND CONVECTION. Geophys. Res. Lett. 35, n/a-n/a. https://doi.org/10.1029/2008GL033190

Harris, A.J.L., Baloga, S.M., 2009. Lava discharge rates from satellite-measured heat flux. Geophys. Res. Lett. 36, L19302. https://doi.org/10.1029/2009GL039717

Harris, A.J.L., Flynn, L.P., Rothery, D.A., Oppenheimer, C., Sherman, S.B., 1999. Mass flux measurements at active lava lakes: Implications for magma recycling. J. Geophys. Res. Solid Earth 104, 7117–7136. https://doi.org/10.1029/98JB02731

Helz, R.T., Clague, D.A., Sisson, T.W., Thornber, C.R., 2014. Petrologic insights into basaltic volcanism at historically active Hawaiian volcanoes (USGS Numbered Series No. 1801–6), Petrologic insights into basaltic volcanism at historically active Hawaiian volcanoes, Professional Paper. U.S. Geological Survey, Reston, VA. https://doi.org/10.3133/pp18016

Holohan, E.P., Schöpfer, M.P.J., Walsh, J.J., 2011. Mechanical and geometric controls on the structural evolution of pit crater and caldera subsidence. J. Geophys. Res. 116, B07202. https://doi.org/10.1029/2010JB008032

Holohan, E.P., Walter, T.R., Schöpfer, M.P.J., Walsh, J.J., van Wyk de Vries, B., Troll, V.R., 2013. Origins of oblique-slip faulting during caldera subsidence: OBLIQUE-SLIP FAULTING AT CALDERAS. J. Geophys. Res. Solid Earth 118, 1778–1794. https://doi.org/10.1002/jgrb.50057

Jackson, M.D., Blundy, J., Sparks, R.S.J., 2018. Chemical differentiation, cold storage and remobilization of magma in the Earth's crust. Nature 564, 405–409. https://doi.org/10.1038/s41586-018-0746-2

Kolzenburg, S., Di Genova, D., Giordano, D., Hess, K.U., Dingwell, D.B., 2018a. The effect of oxygen fugacity on the rheological evolution of crystallizing basaltic melts. Earth Planet. Sci. Lett. 487, 21–32. https://doi.org/10.1016/j.epsl.2018.01.023

Kolzenburg, S., Giordano, D., Cimarelli, C., Dingwell, D.B., 2016. In situ thermal characterization of cooling/crystallizing lavas during rheology measurements and implications for lava flow

653 emplacement. Geochim. Cosmochim. Acta 195, 244–258.
654 https://doi.org/10.1016/j.gca.2016.09.022

655 Kolzenburg, S., Giordano, D., Hess, K.U., Dingwell, D.B., 2018b. Shear Rate-Dependent
656 Disequilibrium Rheology and Dynamics of Basalt Solidification. Geophys. Res. Lett. 45,
657 6466–6475. https://doi.org/10.1029/2018GL077799

658 Kolzenburg, S., Hess, K.-U., Berlo, K., Dingwell, D.B., 2020. Disequilibrium Rheology and
659 Crystallization Kinetics of Basalts and Implications for the Phlegrean Volcanic District.
660 Front. Earth Sci. 8, 187. https://doi.org/10.3389/feart.2020.00187

661 Kumagai, H., 2001. Very-Long-Period Seismic Signals and Caldera Formation at Miyake Island,
662 Japan. Science 293, 687–690. https://doi.org/10.1126/science.1062136

663 Lamy-Chappuis, B., Heinrich, C.A., Driesner, T., Weis, P., 2020. Mechanisms and patterns of
664 magmatic fluid transport in cooling hydrous intrusions. Earth Planet. Sci. Lett. 535,
665 116111. https://doi.org/10.1016/j.epsl.2020.116111

666 Lejeune, A.-M., Richet, P., 1995. Rheology of crystal-bearing silicate melts: An experimental study
667 at high viscosities. J. Geophys. Res. Solid Earth 100, 4215–4229.
668 https://doi.org/10.1029/94JB02985

669 Lev, E., Ruprecht, P., Oppenheimer, C., Peters, N., Patrick, M., Hernández, P.A., Spampinato, L.,
670 Marlow, J., 2019. A global synthesis of lava lake dynamics. J. Volcanol. Geotherm. Res.
671 381, 16–31. https://doi.org/10.1016/j.jvolgeores.2019.04.010

672 Marsh, B.D., 1981. On the crystallinity, probability of occurrence, and rheology of lava and magma.
673 Contrib. Mineral. Petrol. 78, 85–98. https://doi.org/10.1007/BF00371146

674 Métrich, N., Allard, P., Aiuppa, A., Bani, P., Bertagnini, A., Shinohara, H., Parello, F., Di Muro, A.,
675 Garaebiti, E., Belhadj, O., Massare, D., 2011. Magma and Volatile Supply to Post-collapse
676 Volcanism and Block Resurgence in Siwi Caldera (Tanna Island, Vanuatu Arc). J. Petrol. 52,
677 1077–1105. https://doi.org/10.1093/petrology/egr019

678 Michaut, C., Jaupart, C., 2011. Two models for the formation of magma reservoirs by small
679 increments. Tectonophysics 500, 34–49. https://doi.org/10.1016/j.tecto.2009.08.019

680 Michellier, C., Katoto, P. de M.C., Dramaix, M., Nemery, B., Kervyn, F., 2020. Respiratory health
681 and eruptions of the Nyiragongo and Nyamulagira volcanoes in the Democratic Republic
682 of Congo: a time-series analysis. Environ. Health 19, 62. https://doi.org/10.1186/s12940-
683 020-00615-9

684 Michon, L., Massin, F., Famin, V., Ferrazzini, V., Roult, G., 2011. Basaltic calderas: Collapse
685 dynamics, edifice deformation, and variations of magma withdrawal. J. Geophys. Res.
686 116, B03209. https://doi.org/10.1029/2010JB007636

687 Moore, C., Wright, T., Hooper, A., Biggs, J., 2019. The 2017 Eruption of Erta 'Ale Volcano, Ethiopia:
688 Insights Into the Shallow Axial Plumbing System of an Incipient Mid-Ocean Ridge.
689 Geochem. Geophys. Geosystems 20, 5727–5743.
690 https://doi.org/10.1029/2019GC008692

691 Morrison, A., Whittington, A., Smets, B., Kervyn, M., Sehlke, A., 2020. The rheology of crystallizing
692 basaltic lavas from Nyiragongo and Nyamuragira volcanoes, D.R.C. Volcanica 3, 1–28.
693 https://doi.org/10.30909/vol.03.01.0128

694 Naslund, H.R., McBirney, A.R., 1996. Mechanisms of Formation of Igneous Layering, in: Cawthorn,
695 R.G. (Ed.), Developments in Petrology. Elsevier, pp. 1–43. https://doi.org/10.1016/S0167-
696 2894(96)80003-0

697 Neal, C.A., Brantley, S.R., Antolik, L., Babb, J.L., Burgess, M., Calles, K., Cappos, M., Chang, J.C.,
698 Conway, S., Desmither, L., Dotray, P., Elias, T., Fukunaga, P., Fuke, S., Johanson, I.A.,
699 Kamibayashi, K., Kauahikaua, J., Lee, R.L., Pekalib, S., Miklius, A., Million, W., Moniz, C.J.,
700 Nadeau, P.A., Okubo, P., Parcheta, C., Patrick, M.R., Shiro, B., Swanson, D.A., Tollett, W.,
701 Trusdell, F., Younger, E.F., Zoeller, M.H., Montgomery-Brown, E.K., Anderson, K.R.,
702 Poland, M.P., Ball, J.L., Bard, J., Coombs, M., Dietterich, H.R., Kern, C., Thelen, W.A.,
703 Cervelli, P.F., Orr, T., Houghton, B.F., Gansecki, C., Hazlett, R., Lundgren, P., Diefenbach,
704 A.K., Lerner, A.H., Waite, G., Kelly, P., Clor, L., Werner, C., Mulliken, K., Fisher, G., Damby,
705 D., 2019. The 2018 rift eruption and summit collapse of Kīlauea Volcano. Science 363,
706 367–374. https://doi.org/10.1126/science.aav7046

707 Nicholson, R., 1994. Structural Geology by R. J. Twiss and E. M. Moores. W. H. Freeman & Co., San
708 Francisco, 1992. No. of pages: 532. Price: $47.95 (hardback). ISBN 0 7167 2252 6 . Geol. J.
709 29, 382–383. https://doi.org/10.1002/gj.3350290408

710 Patrick, M., Swanson, D., Orr, T., 2019. A review of controls on lava lake level: insights from
711 Halema'uma'u Crater, Kīlauea Volcano. Bull. Volcanol. 81, 13.
712 https://doi.org/10.1007/s00445-019-1268-y

713 Pouclet, A., 1975. Activités du volcan Nyamuragira (Rift ouest de l'Afrique Centrale), évaluation
714 des volumes de matériaux émis. Bull. Volcanol. 39, 466–478.
715 https://doi.org/10.1007/BF02597267

716 Pouclet, A., Bram, K., 2021. Nyiragongo and Nyamuragira: a review of volcanic activity in the Kivu
717 rift, western branch of the East African Rift System. Bull. Volcanol. 83, 10.
718 https://doi.org/10.1007/s00445-021-01435-6

719 R. Hoier, 1939. Contribution à l'étude de la morphologie du volcan Nyamuragira. Exploration du
720 Parc National Albert: Institut des parcs nationaux du Congo Belge.

721 Roche, O., Druitt, T.H., 2001. Onset of caldera collapse during ignimbrite eruptions. Earth Planet.
722 Sci. Lett. 191, 191–202. https://doi.org/10.1016/S0012-821X(01)00428-9

723 Roche, O., Druitt, T.H., Merle, O., 2000. Experimental study of caldera formation. J. Geophys. Res.
724 Solid Earth 105, 395–416. https://doi.org/10.1029/1999JB900298

725 Schultz, R.A., 1995. Limits on strength and deformation properties of jointed basaltic rock masses.
726 Rock Mech. Rock Eng. 28, 1–15. https://doi.org/10.1007/BF01024770

727 Shelly, D.R., Thelen, W.A., 2019. Anatomy of a Caldera Collapse: Kīlauea 2018 Summit Seismicity
728 Sequence in High Resolution. Geophys. Res. Lett. 46, 14395–14403.
729 https://doi.org/10.1029/2019GL085636

730 Simakin, A.G., Trubitsyn, V.P., 1995. Structural evolution of a cooling magma chamber. Izv. Phys.
731 SOLID EARTH CC Fiz. ZEMLI-Ross. Akad. NAUK 31, 132–144.

732 Smets, B., D'Oreye, N., Kervyn, F., 2014. Toward Another Lava Lake in the Virunga Volcanic Field?
733 Eos Trans. Am. Geophys. Union 95, 377–378. https://doi.org/10.1002/2014EO420001

734 Smets, B., Kervyn, M., d'Oreye, N., Kervyn, F., 2015. Spatio-temporal dynamics of eruptions in a
735 youthful extensional setting: Insights from Nyamulagira Volcano (D.R. Congo), in the
736 western branch of the East African Rift. Earth-Sci. Rev. 150, 305–328.
737 https://doi.org/10.1016/j.earscirev.2015.08.008

738 Smith, G.D., Smith, G.D., Smith, S., Gordon Dennis, 1985. Numerical Solution of Partial Differential
739 Equations: Finite Difference Methods. Clarendon Press.

740 Smith, R.L., Bailey, R.A., 1968. Resurgent Cauldrons, in: Geological Society of America Memoirs.
741 Geological Society of America, pp. 613–662. https://doi.org/10.1130/MEM116-p613

742 Sparks, R.S.J., Annen, C., Blundy, J.D., Cashman, K.V., Rust, A.C., Jackson, M.D., 2019. Formation
743 and dynamics of magma reservoirs. Philos. Trans. R. Soc. Math. Phys. Eng. Sci. 377,
744 20180019. https://doi.org/10.1098/rsta.2018.0019

745 Sparks, R.S.J., Huppert, H.E., 1984. Density changes during the fractional crystallization of basaltic
746 magmas: fluid dynamic implications. Contrib. Mineral. Petrol. 85, 300–309.
747 https://doi.org/10.1007/BF00378108

748 Swanson, D.A., Duffield, W.A., Jackson, D.B., Peterson, D.W., 1979. Chronological narrative of the
749 1969-71 Mauna Ulu eruption of Kilauea Volcano, Hawaii (Report No. 1056), Professional
750 Paper. https://doi.org/10.3133/pp1056

751 Tedesco, D., Vaselli, O., Papale, P., Carn, S.A., Voltaggio, M., Sawyer, G.M., Durieux, J., Kasereka,
752 M., Tassi, F., 2007. January 2002 volcano-tectonic eruption of Nyiragongo volcano,
753 Democratic Republic of Congo. J. Geophys. Res. 112, B09202.
754 https://doi.org/10.1029/2006JB004762

755 Ukawa, M., Fujita, E., Ueda, H., Kumagai, T., Nakajima, H., Morita, H., 2006. Long-term geodetic
756 measurements of large scale deformation at Iwo-jima caldera, Japan. J. Volcanol.
757 Geotherm. Res. 150, 98–118. https://doi.org/10.1016/j.jvolgeores.2005.07.008

758 Valade, S., Ley, A., Massimetti, F., D'Hondt, O., Laiolo, M., Coppola, D., Loibl, D., Hellwich, O.,
759 Walter, T.R., 2019. Towards Global Volcano Monitoring Using Multisensor Sentinel
760 Missions and Artificial Intelligence: The MOUNTS Monitoring System. Remote Sens. 11,
761 1528. https://doi.org/10.3390/rs11131528

762 Valade, S., Ripepe, M., Giuffrida, G., Karume, K., Tedesco, D., 2018. Dynamics of Mount
763 Nyiragongo lava lake inferred from thermal imaging and infrasound array. Earth Planet.
764 Sci. Lett. 500, 192–204. https://doi.org/10.1016/j.epsl.2018.08.004

765 Wadge, G., Burt, L., 2011. Stress field control of eruption dynamics at a rift volcano: Nyamuragira,
766 D.R.Congo. J. Volcanol. Geotherm. Res. 207, 1–15.
767 https://doi.org/10.1016/j.jvolgeores.2011.06.012

768 Wadge, G., Cole, P., Stinton, A., Komorowski, J.-C., Stewart, R., Toombs, A.C., Legendre, Y., 2011.
769 Rapid topographic change measured by high-resolution satellite radar at Soufriere Hills
770 Volcano, Montserrat, 2008–2010. J. Volcanol. Geotherm. Res. 199, 142–152.
771 https://doi.org/10.1016/j.jvolgeores.2010.10.011

772 Walker, G.P.L., 1988. Three Hawaiian calderas: An origin through loading by shallow intrusions? J.
773 Geophys. Res. Solid Earth 93, 14773–14784. https://doi.org/10.1029/JB093iB12p14773

774 Wauthier, C., Cayol, V., Poland, M., Kervyn, F., d'Oreye, N., Hooper, A., Samsonov, S., Tiampo, K.,
775 Smets, B., 2013. Nyamulagira's magma plumbing system inferred from 15 years of InSAR.
776 Geol. Soc. Lond. Spec. Publ. 380, 39–65. https://doi.org/10.1144/SP380.9

777 Worster, M.G., Huppert, H.E., Sparks, R.S.J., 1993. The crystallization of lava lakes. J. Geophys. Res.
778 98, 15891. https://doi.org/10.1029/93JB01428

779 Wright, T.L., Marsh, B., 2016. Quantification of the intrusion process at Kīlauea volcano, Hawai'i.
780 J. Volcanol. Geotherm. Res. 328, 34–44.
781 https://doi.org/10.1016/j.jvolgeores.2016.09.019

782 Wright, T.L., Peck, D.L., Shaw, H.R., 1976. Kilauea lava lakes: Natural laboratories for study of
783 cooling, crystallization, and differentiation of basaltic magma. Wash. DC Am. Geophys.
784 Union Geophys. Monogr. Ser. 19, 375–390. https://doi.org/10.1029/GM019p0375

785